Published in final edited form as:
Cell Immunol. 2009 ; 254(2): 94–104. doi:10.1016/j.cellimm.2008.07.002.

Mycobacterium bovis BCG decreases MHC-II expression *in vivo* on murine lung macrophages and dendritic cells during aerosol infection

Nicole D. Pecora[1], **Scott A. Fulton**[2], **Scott M. Reba**[2], **Michael G. Drage**[1], **Daimon P. Simmons**[1], **Nancy J. Urankar-Nagy**[1], **W. Henry Boom**[2,*], and **Clifford V. Harding**[1,*]

1 *Department of Pathology, Case Western Reserve University, Cleveland, Ohio, USA*

2 *Division of Infectious Diseases and Tuberculosis Research Unit, Case Western Reserve University, Cleveland, Ohio, USA*

Abstract

Mycobacterium tuberculosis and *M. bovis* BCG infect APCs. *In vitro*, mycobacteria inhibit IFN-gamma-induced MHC-II expression by macrophages, but the effects of mycobacteria on lung APCs *in vivo* remain unclear. To assess MHC-II expression on APCs infected *in vivo*, mice were aerosol-infected with GFP-expressing BCG. At 28 d, ~1% of lung APCs were GFP+ by flow cytometry and CFU data. Most GFP+ cells were $CD11b^{high}/CD11c^{neg\text{-}mid}$ lung macrophages (58–68%) or $CD11b^{high}/CD11c^{high}$ DCs (28–31%). Lung APC MHC-II expression was higher in infected mice than naïve mice. Within infected lungs, however, MHC-II expression was lower in GFP+ cells than GFP− cells for both macrophages and DCs. MHC-II expression was also inhibited on purified lung macrophages and DCs that were infected with BCG *in vitro*. Thus, lung APCs that harbor mycobacteria *in vivo* have decreased MHC-II expression relative to uninfected APCs from the same lung, possibly contributing to evasion of T cell responses.

Keywords

Mycobacterium; macrophage; dendritic cell; MHC; antigen presentation

Introduction

In vitro studies show that prolonged infection of macrophages with *Mycobacterium tuberculosis* (Mtb) or *M. bovis* BCG (BCG) inhibits IFN-gamma-induced expression of class II transactivator (CIITA) and MHC-II [1;2;3;4;5;6;7], as well as a subset of other IFN-gamma-induced genes [3;7;8], and results in decreased MHC-II antigen presentation [1;2;4;5;6;9]. This mechanism has been demonstrated with murine bone marrow-derived macrophages [1;2;4;7], murine alveolar macrophages [5] and human monocyte-derived macrophages and THP-1 cells [6;9]. Inhibition of CIITA and MHC-II is dependent on Toll-like receptor 2 (TLR2) signaling and can be reproduced with purified Mtb components, such as triacylated lipoproteins, which

Address correspondence to: Clifford Harding, Department of Pathology, Wolstein 6534, Case Western Reserve University, 10900 Euclid Avenue, Cleveland, OH 44106-7288, USA; Phone, 1-216-368-5059; Fax, 1-216-368-0494; Email: cvh3@cwru.edu.
*Joint senior authorship.

are TLR2 ligands [1;2;7;9;10;11]. The inhibition involves blockade of IFN-gamma-induced chromatin remodeling at the CIITA promoter [12]. These mechanisms may contribute to immune evasion and persistence of Mtb by decreasing presentation of Mtb antigens by infected APCs.

In contrast to the *in vitro* studies discussed above, *in vivo* studies using mouse models of mycobacterial infection have provided a more complex picture of the effect of mycobacterial infection on MHC-II expression. Most *in vivo* studies have not distinguished the small proportion of APCs that are directly infected from the large proportion of uninfected APCs that are present in the infected tissue. *In vivo*, T cell responses generate IFN-gamma, which induces MHC-II expression by macrophages. Therefore, macrophage expression of MHC-II may be increased except in the small proportion of macrophages that actually harbor mycobacteria, in which mycobacterial inhibition of MHC-II may be manifested. Indeed, overall MHC-II expression is increased on cells from inflammatory exudates induced by mycobacterial infection (e.g. 12 d after i.p. infection with BCG) [13], but this does not reveal the level of MHC-II expression by the small proportion of such cells that are actually infected by mycobacteria.

This study reports analyses of lung APCs from mice that were aerosol-infected with GFP-expressing *M. bovis*-BCG (BCG-GFP) to allow both the identification of cell types that are infected and the comparison of infected vs. uninfected APCs from the same lung. Aerosol infection recapitulates the natural route of mycobacterial infection, and BCG infection of mice provides a good model of mycobacterial infection with a clinical course similar to that observed of pulmonary infection of humans with Mtb that progresses to latent infection. After aerosol infection of mice with BCG, bacterial burden increases to a peak at 4–5 weeks and then subsides to low or undetectable levels of bacteria (in contrast, infection of mice with virulent Mtb produces a progressive infection with much higher and more persistent bacterial burdens). Following aerosol infection of mice with BCG-GFP, sufficient numbers of infected APCs for our studies were present only near the peak of infection (e.g. 4 weeks), at which time ~1% of all CD11b+ and/or CD11c+ “lung APCs” harbored mycobacteria. APC subsets were defined by their CD11b and CD11c expression pattern, as adapted from the definitions of Gonzalez-Juarrero [14]. Most cells harboring BCG-GFP were $CD11b^{high}/CD11c^{neg\text{-}mid}$ lung macrophages, but $CD11b^{high}/CD11c^{high}$ DCs were also infected. Bacteria were scarcely found in $CD11b^{neg\text{-}low}/CD11c^{mid\text{-}high}$ alveolar macrophages at this time point. Without distinguishing GFP+ and GFP− events, MHC-II levels increased upon infection on all three APC subsets (to varying degrees and not always with statistical significance), but this analysis reflects the uninfected APCs that make up 99% of the APCs within infected lungs. When GFP + and GFP− cells from infected lungs were compared, both GFP+ lung macrophages and GFP + lung DCs had lower MHC-II expression than GFP− cells of these types. Thus, lung macrophages and DCs that harbor mycobacteria have decreased MHC-II expression relative to uninfected macrophages and DCs from the same lung, confirming a mechanism for inhibition of MHC-II expression by mycobacteria *in vivo*.

Materials and Methods

Bacteria

M. bovis BCG, Connaught (ATCC 35745, Manassas, VA) was transformed with plasmid pMV262 [15] (kindly provided by Joel Ernst, New York University, New York, NY) by electroporation (2.5 kV, 800 Ohms, 25 μF) to make BCG-GFP. Transformants were grown on Difco 7H11 agar (BD Biosciences, Franklin Lakes, NJ) in the presence of 30 μg/ml kanamycin (Sigma, St. Louis, MO) at 37°C. The same medium was used for culture of lung homogenates to determine colony-forming unit (CFU) counts over the course of infection. During plating of lung homogenates to determine CFU, lung cells were not intentionally lysed; therefore, a

lung cell harboring more than one BCG bacillus may have produced only a single colony, assuming a lack of spontaneous cell lysis and release of BCG. The pMV262 plasmid is stably maintained by BCG even in the absence of kanamycin for at least 28 d in an infected mouse as indicated by similar CFU counts from lung lysates plated on selective versus non-selective medium.

In vitro infection of bone marrow-derived macrophages

Femur marrow was obtained from female C57BL/6J mice (The Jackson Laboratory, Bar Harbor, ME), which were 6–12 weeks old and housed under specific pathogen-free conditions. To produce macrophages, bone marrow cells were cultured for 7–12 d in standard medium (composed of DMEM (HyClone, Logan, UT) with 10% heat-inactivated FCS (HyClone), 50 μM 2-ME, 2 mM L-glutamine, 1 mM sodium pyruvate, 10 mM HEPES, pH 7.4), which was supplemented with antibiotics and 25% cell-conditioned medium from the LADMAC cell line, which provides M-CSF [16]. Prior to infection, macrophages were plated at 100,000 cells/well in a 96-well plate and cultured overnight in standard medium without LADMAC or antibiotics (unsupplemented standard medium). Bacteria were prepared from freezer stocks by thawing at 37°C, resuspension in unsupplemented standard medium, and passage through a 26-gauge needle 10 times to disrupt clumps of bacteria. Remaining clumps were removed by centrifugation at 200 × *g* for 2 min. Bacteria were added to macrophages at MOI ranging from 0:1 to 40:1 (bacterium:macrophage) for 2 h at 37°C. After 2 h, any non-phagocytosed bacteria were removed from the plates by washing with unsupplemented standard medium. Macrophages and bacteria were incubated at 37°C for an additional 46 h, the last 24 of which were in the presence of 2 ng/ml IFN-gamma, and then assessed with antigen processing assays or flow cytometry.

Antigen presentation by bone marrow-derived macrophages

Soluble ovalbumin (OVA, Sigma) or OVA(323-339) peptide was added to macrophages for 2 h. Cells were washed in DMEM and fixed in 0.5% paraformaldehyde in PBS. DOBW T hybridoma cells, which recognize OVA(323-339):I-A^d or OVA(323-339):I-A^b complexes, were added (100,000 cells/well) for 24 h. IL-2 in the supernatant was measured by a colorimetric CTLL-2 bioassay. Supernatants (100 μl) were combined with 5000 CTLL-2 cells in 100 μl and incubated for 24 h. Alamar Blue (Trek Diagnostic Systems, Cleveland, OH) was added for 24–48 h, and a Bio-Rad Model 550 microplate reader was used to determine OD_{550}–OD_{595}.

Aerosol infection of mice and preparation of lung APCs

BCG-GFP cultures were prepared by adding 1.5×10^8 bacteria to 150 ml of 7H9 medium (Difco) with 30 μg/ml kanamycin. Cultures were grown with shaking for 5 d at 37°C. Bacteria were harvested at approximately mid-log phase by centrifugation (1800 × *g*, 15 min) and resuspended in 10 ml sterile LPS-free water (Invitrogen, Carlsbad, CA). Bacterial clumps were disrupted by three sequential aspirations through a sterile 26-gauge hypodermic needle, and 10 ml of the suspension was placed in the glass nebulizer chamber of the Inhalation Exposure System (Glas Col, Terre Haute, IN). Female C57BL/6J mice (8–16 weeks old, Jackson Laboratory, Bar Harbor, ME) were exposed to bacterial aerosol for 50 min with input and output airflow rates set at 7 l/min and 24 l/min, respectively. The number of BCG-GFP implanted in the lung was determined 1 d after infection by culturing lung homogenate. On average, 2000–4000 CFU were present in the combined, lavaged lungs of each mouse.

After 28–33 d of infection, mice were anesthetized with 750 μl of 1.25% 2,2,2 tribromoethanol (Sigma, T4840-2) in 40% 2-methyl-2-butanol (tert-amyl alcohol; Sigma, A-1685) i.p. and exsanguinated by cutting the renal arteries. The diaphragm and the lower ribcage were removed to expose the lungs, surrounding tissue was removed to expose the trachea, and an incision (1

mm) was made in the trachea just below the first tracheal ring. An 18-gauge angiocatheter (BD Biosciences) was inserted to lavage the lungs 3 times with 1 ml of sterile PBS to produce 3 ml of bronchoalveolar lavage (BAL) fluid from each mouse. After lavage, lungs were removed, minced in a glass Petri dish and incubated for 60–90 min at 37°C with rotation in 2.5 mg/ml collagenase D (Roche, Indianapolis, IN) in RPMI (HyClone) supplemented with 10% fetal bovine serum (FBS) (Hyclone). The suspension was forced through a 70-μm filter and pelleted at 450 × *g* for 5 min. The supernatant was decanted, the pellet was resuspended in erythrocyte lysis buffer (0.01 M Tris-HCl, 0.16 M NH_4Cl, pH 7.3) for 5 min, and the suspension was pelleted at 450 × *g* for 5 min. The pellet was resuspended in PBS with 0.5% BSA and passed over a 40-μm filter to yield "total lung homogenate". For experiments involving detection of GFP+ events, cells were incubated with magnetic beads coated with anti-CD11b or anti-CD11c (Miltenyi, Auburn, CA), washed and eluted according to the manufacturer's instructions to produce "CD11b affinity-sorted cells" or "CD11c affinity-sorted cells". Cells from 2–10 mice within an experimental group were pooled to produce BAL, total lung homogenate, CD11b affinity-sorted cells or CD11c affinity-sorted cells. Samples of BAL, total lung homogenate, CD11b affinity-sorted cells or CD11c affinity-sorted cells were cultured to determine bacterial load (CFU).

Flow cytometry

BAL cells, total lung homogenate cells, CD11b affinity-sorted cells or CD11c affinity-sorted cells were washed in PBS with 0.1% BSA and incubated for 30 min on ice in the same buffer with 1:100 anti-CD16/CD32 (Pharmingen, BD Biosciences, San Jose, CA) to block Fc receptors. Cells were then stained with one of 2 sets of antibodies. The first set consisted of anti-CD11b-APC-CY7 (Pharmingen, #557657), anti-CD11c-Pacific Blue (eBioscience, #57-0114-82, San Diego, CA) and anti-MHC-II-APC (eBioscience, #17-5321-82). The second set (used before the first set of antibodies was available), consisted of anti-CD11b-APC-CY7, anti-CD11c-APC (eBioscience, #17-0114) and anti-MHC-II (Y3P-biotin). The second set required a second incubation with streptavidin-Pacific Blue (Molecular Probes, #S11222) for 30 min on ice. Use of CD11b- or CD11c-conjugated magnetic beads for preparation of cells does not prevent subsequent staining for those markers by fluorochrome-tagged antibodies of the same clone (manufacturer's protocol, Miltenyi). Cells were analyzed with an LSR-II (BD Biosciences) or FACsARIA (BD Biosciences) flow cytometer. From the R0 gate (all events), the R1 gate was set to include all events except those with very low forward and side scatter, consistent with subcellular debris. Events in the R1 gate were segregated according to the expression of CD11b and CD11c for inclusion in the R2 ($CD11b^{neg\text{-}low}/CD11c^{mid\text{-}high}$), R3 ($CD11b^{high}/CD11c^{neg\text{-}mid}$) or R4 ($CD11b^{high}/CD11c^{high}$) gate. The majority of cellular autofluorescence falls within the green-yellow spectral region (500–600 nm), the same region as GFP fluorescence. To correct for autofluorescence, events in these populations were plotted on a 2-dimensional histogram to show fluorescence excited by the 488 nm laser at both 575 nm (autofluorescence correction channel) and 525 nm (GFP channel). Events that were shifted toward greater fluorescence in the GFP channel relative to the autofluorescence channel were included in gate R6, and other events were included in gate R5. Thus, BCG-GFP+ cells were shifted into R6 relative to BCG-GFP− cells with similar autofluorescence profiles that were present in R5.

Flow cytometry data were analyzed with WinList software (Verity Software House, Topsham, ME). MFIs represent linear means of events from a specified gated cell population from a single experiment. The percentage of events within a gate is expressed as the mean +/− standard deviation (SD) of results from 3–4 replicate experiments, each containing 2–10 mice, unless a single representative experiment is explicitly presented. MHC-II expression by different cell subsets was assessed by comparing the mean MFI values for different groups (e.g. BCG-GFP + vs. BCG-GFP−) from multiple experiments with groups from a single experiment paired.

MFI data from multiple experiments were summarized by mean and standard error of the mean (SEM). The difference of MFI between two groups was examined by paired T-test. All tests were two-sided, and p-value ≤ 0.05 was considered statistically significant.

Microscopy

Cells from gate R6 were sorted onto microscope slides with a FACSAria to confirm their infection and count the number of bacilli per cell. Cells were mounted in ProLong Gold anti-fade medium (Molecular Probes) containing DAPI. Images shown were generated with a Zeiss LSM510 inverted confocal microscope system using a Plan-Apochromat 63x/1.4 oil DIC objective with a 2x zoom. For scoring cells, a Leica DM LB fluorescence microscope with a 100X objective was employed.

Antigen presentation by purified lung APCs

Homogenates were prepared from post-lavaged lungs of 20 naïve BALB/c mice as described above, dead cells and tissue debris were removed using a dead cell removal kit (Miltenyi), and CD11c affinity-sorted cells were prepared as described above. A FACsAria flow cytometer (BD Biosciences) was used to sort APCs by CD11b and CD11c expression, typically yielding 10^6 alveolar macrophages, 5–8 × 10^5 lung macrophages and 10^5 dendritic cells. Purified lung APCs were incubated in 96-well plates (50,000–75,000/well for alveolar and lung macrophages; 50,000 cells/well for lung DCs) in standard medium for 24 h and then with or without BCG-GFP for an additional 48 h, the last 24 h of which was with 4 ng/ml IFN-gamma. Soluble endotoxin-free OVA (Profos AG, Germany) was then added at 1 mg/ml for 24 h with fresh IFN-gamma (4 ng/ml). Cells were washed, fixed in paraformaldehyde, washed and incubated with DOBW cells as described above. IL-2 was measured by ELISA.

Results

Flow cytometry detection of bone marrow-derived macrophages infected with BCG-GFP in vitro

To establish a method for distinguishing mycobacteria-infected cells from uninfected cells, we expressed GFP in BCG, and the resulting BCG-GFP bacteria were used to infect mice or cell cultures. Transformation of BCG with the GFP-expressing plasmid pMV262 increased bacterial MFI approximately twenty-fold over background (Fig. 1A) to a level exceeding the background MFI of bone marrow-derived macrophages (Fig. 1B). To test detection of cells infected with BCG-GFP, bone marrow-derived macrophages were incubated with BCG-GFP for 48 h at varying MOI (IFN-gamma was added for the last 24 h), and the cells were analyzed by flow cytometry (Fig. 1B). With MOI of 5:1, BCG-GFP-infected cells were readily detectable with a shift in fluorescence. At MOI of 40:1 most bone marrow-derived macrophages were infected, as manifested by increased MFI, and MHC-II expression was decreased by 2-fold (Fig. 1C, D). In addition, BCG-GFP caused a dose-dependent decrease in the ability of bone marrow-derived macrophages to process OVA and present it to DOBW T hybridoma cells (Fig. 1E). These results indicate that BCG-GFP inhibits MHC-II expression and antigen processing/presentation, consistent with earlier studies with Mtb [1;2;3]. Furthermore, cells harboring BCG-GFP were detected by flow cytometry in this *in vitro* system, allowing us to further test this approach for *ex vivo* analysis of cells infected *in vivo* in the course of pulmonary mycobacterial infection.

Infection with BCG-GFP increases numbers of CD11b^{high}/CD11c^{high} cells in the lung

The main goal of this study was to compare the expression of MHC-II by BCG-infected vs. uninfected APCs from the same lungs. As a foundation to achieve this primary goal, we first characterized the lung APC subsets that were present with or without aerosol infection with

BCG. Lungs of naïve mice were lavaged to remove alveolar macrophages, which were analyzed separately, and lungs were then minced, digested with collagenase, and passed through a 40-μm filter to create a single cell suspension ("total lung homogenate"). Cells were stained for CD11b and CD11c for flow cytometry (Fig. 2A). From all events (R0 gate), the R1 gate was set to include all R0 events except those with very low forward and side scatter consistent with subcellular debris (Fig. 2B). From R1, events were gated into the $CD11b^{neg\text{-}low}/CD11c^{mid\text{-}high}$ (R2), $CD11b^{high}/CD11c^{neg\text{-}mid}$ (R3) or $CD11b^{high}/CD11c^{high}$ (R4) gate (Fig. 2B). Lung APC subsets were defined as in previous studies [14;17], characterizing $CD11b^{neg\text{-}low}/CD11c^{mid\text{-}high}$ cells (gate R2) as alveolar macrophages (in BAL or post-lavage residual alveolar macrophages in lung), $CD11b^{high}/CD11c^{neg\text{-}mid}$ cells (gate R3) as lung macrophages, and $CD11b^{high}/CD11c^{high}$ cells (gate R4) as DCs (Table 1). These definitions are useful to distinguish major APC subsets in a manner consistent with prior studies, although they are approximations, given the array of APC phenotypes and the limited resolution of subsets by expression of CD11b and CD11c alone. Although it is useful to analyze these subsets separately for some purposes, our subsequent conclusions regarding changes in MHC-II expression are not dependent on isolation of single APC types by this approach.

Within homogenates of lavaged naïve mouse lungs, $CD11b^{high}/CD11c^{neg\text{-}mid}$ lung macrophages were the most abundant APC subset (Fig. 2B, C), representing 29.7 +/− 3.4% of cells in R1 and 71.1 +/− 2.5% of total lung APCs (R2 + R3 + R4) (numbers represent mean +/− SD for three independent experiments). $CD11b^{high}/CD11c^{high}$ DCs accounted for 3.2 +/− 1.2% of cells in R1 and 7.5 +/− 2.3% of total lung APCs, and $CD11b^{neg\text{-}low}/CD11c^{mid\text{-}high}$ alveolar macrophages were 9.1 +/− 1.9% of cells in R1 and 21.7 +/− 3.8% of total lung APCs. Analysis of BAL from naïve mice showed that 69.7 +/− 4.1% of BAL cells belonged to the $CD11b^{neg\text{-}low}/CD11c^{mid\text{-}high}$ subset, 3.4 +/− 2.6% were in the $CD11b^{high}/CD11c^{high}$ subset, and 0.8 +/− 0.6% were in the $CD11b^{high}/CD11c^{neg\text{-}mid}$ subset. The remainder of both the lung homogenate and the BAL consisted of $CD11b^{negative}/CD11c^{negative}$ cells.

To characterize APCs from BCG-infected lungs, C57BL/6J mice were aerosol-infected with BCG, an established model for pulmonary mycobacterial infection [18;19;20], to achieve 300–400 CFU in the BAL and 2000–4000 CFU in the post-lavage lung tissue as assessed 1 d after infection. Bacterial loads peaked at 4–5 weeks post-infection, with $1.7 \times 10^4 – 7.5 \times 10^4$ CFU per set of lavaged mouse lungs, and then declined, as previously described [18]. After aerosol infection of mice, BCG achieves pulmonary bacterial loads that are much lower than those achieved with virulent Mtb, and sufficient numbers of infected APCs for our studies were obtained only near the peak of infection (~4 weeks). Therefore, mice were sacrificed 28–33 d after aerosol infection with BCG-GFP, and lung cells were prepared for flow cytometry (Fig. 2A). Our initial analysis addressed changes in lung APCs and their expression of CD11b and CD11c without measuring GFP signal (Fig. 2B, C). Of APCs isolated from lung tissue, BCG infection increased $CD11b^{high}/CD11c^{high}$ cells from 3.2 +/− 1.2% to 7.5 +/− 2.3% of R1 total lung homogenate cells (average of 3 experiments), whereas $CD11b^{neg\text{-}low}/CD11c^{mid\text{-}high}$ cells decreased from 9.1 +/− 1.9 % to 4.3 +/− 2.2% of R1 cells. The $CD11b^{high}/CD11c^{neg\text{-}mid}$ subset was essentially unchanged with infection, representing 29.7 +/− 3.4% and 29.5 +/− 7.0% of R1 cells from naïve and BCG-GFP-infected mice, respectively. Within the BAL, BCG infection expanded the $CD11b^{high}/CD11c^{high}$ subset from 3.4 +/− 2.6% to 22.5 +/− 5.8% of R1 BAL cells, whereas the $CD11b^{neg\text{-}low}/CD11c^{mid\text{-}high}$ subset decreased from 69.7 +/− 4.1% to 57.3 +/− 3.3% of R1 BAL cells, and the $CD11b^{high}/CD11c^{neg\text{-}mid}$ subset increased from 0.8 +/− 0.6% to 2.9 +/− 2.5% of R1 BAL cells. In summary, infection with BCG increased the proportion of $CD11b^{high}/CD11c^{high}$ DCs in both the lung and the BAL, while the proportion of $CD11b^{high}/CD11c^{neg\text{-}mid}$ lung macrophages remained constant in the lung and increased within the BAL and the proportion of $CD11b^{neg\text{-}low}/CD11c^{mid\text{-}high}$ alveolar macrophages declined in both lung and BAL.

Ex vivo flow cytometry detection of infected lung APCs following in vivo aerosol-induced pulmonary infection with BCG-GFP

To study APCs that harbored mycobacteria *in vivo*, lungs were harvested 28–33 d after aerosol infection with BCG-GFP. Immunoaffinity isolation with anti-CD11b or anti-CD11c magnetic beads was used to enrich APCs and remove contaminating lung cell populations with high autofluorescence that interfered with detection of GFP (Fig. 3 and subsequent figures). Cells were then stained for CD11b and CD11c for flow cytometry. The R1 gate was used to exclude subcellular debris (Fig. 3A, D), and lung APC subsets were defined from R1 events based on levels of CD11b and CD11c expression (Fig. 3B, E). Total lung APCs (CD11b+ and/or CD11c + cells; R2 + R3 + R4) were then analyzed for GFP signal. Since most lung APCs express at least low levels of both CD11b and CD11c, the cell populations isolated by CD11b and CD11c immunoaffinity sorting were overlapping. Nonetheless, analyses were performed separately on both CD11b and CD11c immunoaffinity-sorted cell samples to avoid potential selection bias due to preferential isolation of APC subsets with higher expression of CD11b or CD11c. The similar results we obtained with the two sorted cell samples provided additional confirmation of our conclusions.

A two-parameter autofluorescence correction method [21;22] was used to detect GFP+ cells, since signal from BCG-GFP was not sufficient to shift fluorescence beyond the widely-spread background autofluorescence of the population on a one-dimensional histogram. Total CD11b + and/or CD11c+ cells (R2 + R3 + R4) from either CD11b or CD11c immunoaffinity-sorted samples were plotted on a two-dimensional histogram to show fluorescence (excited by the blue 488 nm laser) at 575 nm (autofluorescence correction channel) vs. 525 nm (GFP channel). Events that were shifted toward greater fluorescence in the GFP channel relative to the autofluorescence channel were included in gate R6, and other events were included in gate R5 (Fig. 3C, F). The GFP-specific shift in fluorescence appeared smaller than reported by some other groups [17;21], possibly due to smaller numbers of bacteria present after aerosol infection (as opposed to intranasal infection), paraformaldehyde fixation in our protocol, which increases cellular autofluorescence (but is advantageous for biohazard control), or different fluorescence intensity of BCG-GFP strains. GFP+ infected cells were not detected in BAL, perhaps reflecting the low level of infection of alveolar macrophages at this time point and the high autofluorescence of these cells. Of CD11b affinity-sorted total lung APCs (R2 + R3 + R4), the mean proportion of GFP+ events (R6 gate) was 0.60 +/− 0.21% (range of 0.38% to 0.86% over 4 experiments). In CD11c affinity-sorted samples, GFP+ events (R6) represented 0.52 +/− 0.26% (range of 0.21% to 0.82% over 4 experiments) of lung APCs. Overall, these results indicate that BCG-GFP is detected by flow cytometry in approximately 0.6% of lung APCs.

Flow cytometry detection of BCG-GFP-infected cells was validated by several approaches. First, R6 events were enumerated in cells from lungs of naïve mice or mice infected with non-fluorescent BCG. From naïve mice, 0.09 +/− 0.10% (range of 0.02% to 0.24% in 4 experiments) of CD11b affinity-sorted cells and 0.07 +/− 0.02% (range of 0.05% to 0.09% in 4 experiments) of CD11c affinity-sorted cells were in the R6 gate (Fig. 3C), indicating a false positive background of approximately 15% of the signal seen in BCG-GFP-infected mice. From mice that were infected with non-fluorescent BCG, 0.07% of CD11b affinity-sorted and 0.09% of CD11c affinity-sorted cells were in the R6 gate, indicating a 12–17% background. Thus, the background in this assay was only ~15%, and the similar background with naïve and non-fluorescent BCG-infected mice justified subsequent comparison of BCG-GFP-infected and naïve mice.

A second validation approach was to sort R6 events by FACS and then perform fluorescence microscopy (Fig. 4A). Clearly demarcated fluorescent bacteria were present in 55 +/− 23% of CD11b affinity-sorted cells in the R6 gate and 59 +/− 21% of CD11c affinity-sorted cells in the R6 gate (mean +/− SD, 3–4 experiments), and many other cells contained highly fluorescent

granules, apparently representing partially degraded mycobacteria. Thus, most cells in the R6 gate contained BCG-GFP. The majority of CD11b or CD11c affinity-sorted cells in the R6 gate contained 1–5 rods (Fig. 4B), and many contained only a single visible BCG-GFP bacillus, indicating that sensitivity of flow cytometry was sufficient to detect infection with a single bacillus.

A third validation approach was to compare the number of BCG-GFP+ APCs to the number of CFU cultured from infected tissues with both numbers normalized to the number of cells in the starting material. Assuming that each CFU represents one infected cell, the flow cytometry sensitivity (detection efficiency) was 38–42% (Table 2). Since cells that contained more than one bacillus may have produced more than one CFU, the number of infected APCs may have been lower than implied by the CFU analysis, implying a higher flow cytometry detection efficiency than calculated above. Although there are caveats to this sensitivity analysis, it is reassuring that the sensitivities implied by independent CFU and fluorescence microscopy analyses are in reasonable agreement. In summary, APCs that harbor BCG-GFP *in vivo* can be identified by *ex vivo* flow cytometry, allowing subsequent studies to compare infected and uninfected APCs from lungs of mice with pulmonary mycobacterial infection.

$CD11b^{high}/CD11c^{neg\text{-}mid}$ lung macrophages harbor the most bacteria, but a higher proportion of $CD11b^{high}/CD11c^{high}$ lung DCs is infected

Flow cytometry was used to determine which APC subsets harbored bacteria after aerosol infection with BCG-GFP. The $CD11b^{high}/CD11c^{neg\text{-}mid}$ subset contained the largest number of GFP+ events, followed by the $CD11b^{high}/CD11c^{high}$ subset (Fig. 5). Of GFP+ (R6) events derived from CD11b affinity-sorted cells, $CD11b^{high}/CD11c^{neg\text{-}mid}$ cells represented 67.9 +/− 12.9% and $CD11b^{high}/CD11c^{high}$ cells represented 27.5 +/− 13.0% (n = 4 experiments). $CD11b^{neg\text{-}low}/CD11c^{mid\text{-}high}$ cells were too scarce in CD11b affinity-sorted samples for analysis of GFP+ events. Of GFP+ (R6) events derived from CD11c affinity-sorted cells, $CD11b^{high}/CD11c^{neg\text{-}mid}$ cells represented 57.9 +/− 22.6%, $CD11b^{high}/CD11c^{high}$ cells represented 30.9 +/− 16.9%, and $CD11b^{neg\text{-}low}/CD11c^{mid\text{-}high}$ cells were 7.2 +/− 3.9% (higher autofluorescence of this population may have caused an underestimate of the number of infected $CD11b^{neg\text{-}low}/CD11c^{mid\text{-}high}$ cells). Thus, most BCG-GFP-infected APCs were in the $CD11b^{high}/CD11c^{neg\text{-}mid}$ "lung macrophage" subset, and $CD11b^{high}/CD11c^{high}$ DCs were the other major subset of infected cells. Since there are far fewer $CD11b^{high}/CD11c^{high}$ cells than $CD11b^{high}/CD11c^{neg\text{-}mid}$ cells in the lung, a higher proportion of $CD11b^{high}/CD11c^{high}$ DCs was actually infected.

Pulmonary infection increases mean MHC-II expression on lung APCs, but MHC-II is decreased on APCs that harbor mycobacteria

Several groups have demonstrated that infection of macrophages with mycobacteria *in vitro* inhibits expression of MHC-II, a finding that has yet to be demonstrated *in vivo*. To address regulation of MHC-II expression on specific subsets of infected lung APCs, MHC-II expression was assessed on $CD11b^{neg\text{-}low}/CD11c^{mid\text{-}high}$ (R2), $CD11b^{high}/CD11c^{neg\text{-}mid}$ (R3) and $CD11b^{high}/CD11c^{high}$ (R4) lung cells from both naïve and infected mice. Each APC subset was divided into GFP− (R5) and GFP+ (R6) cells and levels of MHC-II expression were assessed. For all three APC subsets the mean MHC-II expression was higher on GFP− (R5) APCs from infected lungs than APCs from naive lungs (data cited below represent mean values from at least three independent experiments +/− SEM). MHC-II expression increased 4.00 +/− 0.49-fold for total R2 cells, 1.24 +/− 0.27-fold for total R3 cells and 1.90 +/− 0.53-fold for total R4 cells ($p < 0.05$ for R2; $p > 0.05$ for R3 and R4). However, GFP+ (R6) cells in the $CD11b^{high}/CD11c^{neg\text{-}mid}$ (R3) and $CD11b^{high}/CD11c^{high}$ (R4) subsets had significantly lower MHC-II levels than GFP− (R5) cells in the same subsets from the same lungs. There was a 1.73 +/− 0.11-fold decrease in MHC-II expression for R3 cells and a 1.70 +/− 0.14-fold

decrease for R4 cells (Fig. 6, $p < 0.05$ for both). There were insufficient numbers of GFP+ R2 events for analysis. On GFP+ APCs from both R3 and R4, MHC-II expression was reduced to a level that was not significantly different from MHC-II expression on cells from naïve mice. In summary, BCG-GFP infection generally increased MHC-II expression on APCs that did not harbor mycobacteria, but MHC-II levels were significantly lower on lung macrophages and dendritic cells that actually harbored BCG-GFP than on uninfected cells of the same APC subsets from the same lungs.

Infection with BCG-GFP in vitro inhibits MHC-II antigen processing and presentation in all lung APC subsets

Although MHC-II levels were significantly lower on BCG-GFP+ macrophages and dendritic cells after infection *in vivo*, flow cytometry studies of cells from infected lungs did not suffice to determine whether MHC-II antigen presentation by lung APCs was functionally inhibited. Since the very low number of BCG-GFP+ cells present in infected lungs precluded isolation of sufficient numbers of in vivo-infected APCs for functional antigen presentation assays, lung APCs were purified from lungs of naïve mice, infected in vitro with BCG-GFP and used in an assay of antigen processing and presentation to determine the functional impact of infection. Infection with BCG-GFP inhibited the ability of all three lung APC subsets, alveolar macrophages, dendritic cells and lung macrophages, to process and present exogenous OVA to DOBW T hybridoma cells (Fig. 7). These data confirm that the reduction in MHC-II expression that results from infection of lung macrophages and DCs *in vivo* is paralleled by an infection-induced functional deficit in antigen processing and presentation function, albeit one that was studied by *in vitro* infection of these purified lung APC subsets.

Discussion

The goals of this study were to develop a method to distinguish lung APCs harboring mycobacteria from uninfected APCs in the same lung and apply this tool to assess direct regulation of APCs by mycobacteria (distinct from regulation by cytokines and other factors present in the infected lung). Mice were aerosol-infected with BCG-GFP. Our study focused exclusively on the peak of infection at ~28 d, when sufficient numbers of BCG-GFP-infected APCs could be isolated for analysis. Mycobacterial inhibition of MHC-II expression may be more pronounced and effective later in the course of infection, but later time points yield too few infected APCs to permit the type of analysis used in this paper. Overall, we observed that MHC-II expression was lower in infected APCs than in uninfected APCs of the same subsets from the same infected lungs. This is a novel *in vivo* demonstration of mycobacteria-induced inhibition of MHC-II, a process that has been studied *in vitro.*

During pulmonary infection, mycobacteria can infect both macrophages and dendritic cells. Following aerosol infection with BCG-GFP (28 d), we observed that most infected cells were $CD11b^{high}/CD11c^{neg\text{-}mid}$ lung macrophages, although a higher percentage of the less abundant $CD11b^{high}/CD11c^{high}$ DCs was infected. Previous studies have shown that after intranasal infection of mice for 48 h with BCG-GFP, 15% of infected cells in the lung had a DC phenotype ($CD11c^{+}/33D1^{+}$), while the rest were categorized as macrophages [21]. In a study by Humphreys et al., Mtb was contained largely within alveolar macrophages at early time points after intranasal infection and then largely within $CD11b^{high}/CD11c^{high}$ DCs at later time points [17]. In other studies with aerosol infection with Mtb, infection of DCs was also prominent [23]. Thus, both macrophages and DCs harbor mycobacteria in the infected lung, and the proportions of infected cell types vary with the time point and infection model.

A great deal of *in vitro* work with both murine and human primary cells and cell lines has shown that IFN-gamma-induced MHC-II expression is decreased on macrophages (including alveolar and bone marrow-derived macrophages) upon infection with mycobacteria or

exposure to mycobacterial components, e.g. lipoproteins LpqH, LprG or LprA, which signal through TLR2 [1;2;3;4;5;6;7;9;10]. The decrease in MHC-II protein expression by macrophages correlates with decreases in the mRNA for MHC-II and CIITA [2;4], which is the master regulator of MHC-II gene transcription. While mycobacteria and TLR agonists increase expression of MHC-II protein on bone marrow-derived DCs [10], this increase reflects post-translational regulation, and these stimuli decrease CIITA and MHC-II mRNA in DCs, like macrophages. Interestingly, our studies suggest that infection with BCG *in vivo* may decrease MHC-II expression on lung DCs, in contrast to results with bone marrow-derived DCs *in vitro*. Mycobacteria also inhibit macrophage expression of other genes that contribute to antigen processing and presentation [7]. As a result, mycobacteria decrease the ability of macrophages to process and present antigens to T cells [1;4]. This process requires mycobacterial infection or stimulation of TLR2 by mycobacterial lipoproteins for ~24 h to allow for a number of events, putatively including TLR2 signaling, induction of negative regulators of CIITA transcription (including C/EBP) [24], chromatin remodeling at the CIITA promoter [12], decreased CIITA transcription and sequential decay of CIITA mRNA, MHC-II mRNA and MHC-II protein expression. In addition to the goal of evaluating MHC-II regulation *in vivo*, this study extends prior experiments to include *in vitro* studies of lung-derived APCs (Fig. 7), demonstrating that MHC-II antigen processing and presentation is inhibited by BCG infection of purified lung macrophages and dendritic cells, as well as alveolar macrophages.

While previous studies of *in vivo* mycobacterial infection have reported an increase in MHC-II expression on macrophages [13;14], these studies did not distinguish the small proportion of macrophages that actually harbored mycobacteria, and it is necessary to distinguish direct regulation of infected macrophages by mycobacteria from regulation of the more numerous uninfected macrophages by cytokines and other regulators that are present in infected tissue (e.g. IFN-gamma that is increased at this time point of infection). Accordingly, we used flow cytometry to discriminate BCG-GFP-infected APCs from uninfected APCs from the same lungs using a method sensitive enough to detect a single BCG-GFP bacillus in an APC. Consistent with prior *in vivo/ex vivo* studies, we observed that infection of mice with BCG-GFP increased MHC-II expression on most lung APCs, but our studies revealed the novel finding that MHC-II expression was lower on GFP+ (infected) cells than on GFP− (uninfected) cells of the same APC subset for both $CD11b^{high}/CD11c^{high}$ DCs and $CD11b^{high}/CD11c^{neg\text{-}mid}$ lung macrophages (we obtained too few GFP+ $CD11b^{neg\text{-}low}/CD11c^{mid\text{-}high}$ alveolar macrophages for this analysis). MHC-II expression was decreased on GFP+ lung macrophages and DCs to levels that were not significantly different from those seen on the same APC subsets from naïve mice.

One issue is the degree of inhibition achieved, since mean MHC-II expression was only partially inhibited in BCG-GFP+ APCs (60% and 59% inhibition relative to GFP− DCs and lung macrophages, respectively). The mean decrease in MHC-II expression may understate the impact of the effect, since the APC subsets defined by expression of CD11b and CD11c are heterogeneous, and minor subsets with greater inhibition of MHC-II may provide important niches for the small numbers of mycobacteria that persist in latent inhibition. In addition, antigen presentation may be inhibited further by mechanisms other than decreased MHC-II expression. Indeed, we observed Mtb-induced defects in expression of multiple genes that contribute to antigen processing or presentation [7], and inhibition of antigen processing and presentation was more profound than the decrement in MHC-II expression [9]. Similarly, Fig. 1E demonstrates that processing and presentation of OVA by bone marrow-derived macrophages is substantially inhibited even at an MOI (e.g. 10:1) that causes only partial inhibition of MHC-II expression, and Fig. 7 shows that BCG infection strongly inhibits antigen processing and presentation function of alveolar macrophages, lung macrophages and lung DCs (functional inhibition again more dramatic than the change in MHC-II expression). We

speculate that even greater inhibition of MHC-II expression may occur during later stages of infection that were not analyzed in our study (due to insufficient bacterial load for BCG-GFP flow cytometry analysis). Thus, a combination of *in vivo* and *in vitro* results suggest that mycobacteria inhibit APC function, contributing to their ability to evade T cell immunity during latent infection.

Other studies have produced various insights into *in vivo* regulation of MHC-II on lung APCs. One study showed that MHC-II levels on $CD11b^{+}CD11c^{high}$ foamy macrophages increased upon acute infection with Mtb but dropped below the level seen on cells from naïve mice in later stages of chronic infection [25]. In another study, acute Mtb infection increased MHC-II expression on all APC subsets except $CD11b^{high}/CD11c^{high}$ DCs, but MHC-II expression by most APC subsets later decreased to levels seen on cells from naïve mice [14]. An immunohistochemical study showed that MHC-II levels were low on macrophages within granulomas that contained Mtb, whereas surrounding DCs had higher MHC-II expression [26]. Recently, Kincaid et al used infection with GFP-expressing Mtb to assess MHC-II levels on infected versus uninfected lung cells from mice infected with Mtb H37Rv. Their studies did not reveal statistically significant changes in MHC-II expression on macrophages, while a small, statistically significant increase in MHC-II expression was present on infected DCs at 21 d after infection but not at 28 or 35 d after infection [27]. Thus, *in vivo* studies have produced varying results with different models, but our data and some other reports suggest that MHC-II expression may be decreased on specific APC subsets at certain times during Mtb infection, even though MHC-II expression may be increased on other APCs or at other time points. Moreover, inhibition of MHC-II expression in even a small proportion of APCs would suffice to provide niches for the small number of Mtb bacilli that persist during chronic infection.

Although TLR2 has been implicated in the inhibition of MHC-II expression, which may allow Mtb to evade immune surveillance, the overall impact of TLRs in mycobacterial disease is to promote the host immune response. In humans, polymorphisms that cause a defect in TLR2 signaling worsen outcomes in both tuberculosis and leprosy [28;29;30], and TLR2 is important for the murine immune response to mycobacterial infection [31;32]. Thus, the predominant role of TLRs in mycobacterial disease is host-beneficial. However, one consequence of prolonged TLR2 signaling is inhibition of MHC-II expression an antigen presentation by macrophages. We propose that this reflects a homeostatic program designed to down-regulate APC function to prevent excessive generation of inflammatory and tissue-damaging effector T cell responses, and this program may be subverted by Mtb (and perhaps other intracellular pathogens that persist in APCs). Thus, mycobacteria that survive and signal though TLR2 in host cell phagosomes may use the host's own anti-inflammatory homeostatic negative feedback mechanism to inhibit APC function of the infected macrophage and establish a niche for evasion of immune surveillance.

In summary, our results provide a novel demonstration that MHC-II expression is inhibited *in vivo* in cells that directly harbor mycobacteria despite increased MHC-II expression by other APCs of the same subsets in the same infected lungs. These results provide important *in vivo* validation for *in vitro* studies of the ability of mycobacteria to inhibit MHC-II expression and antigen presentation. We propose that mycobacteria evade immune surveillance by CD4+ T cells by persisting in niches provided by APCs in which direct mycobacterial signaling inhibits expression of MHC-II and other proteins required for Ag processing and presentation.

Acknowledgements

This work was supported by NIH grants AI035726, AI034343 and AI069085 to CVH and AI27243 and HL55967 to WHB. Experiments using mice were approved by the Institutional Animal Care and Use Committee of Case Western Reserve University (protocol 2005-0129). The authors have no financial conflicts of interest. We thank Piet de Boer and Rob Fairchild for scientific advice and assistance, Joel Ernst for providing the pMV262 plasmid, Pingfu Fu (Case

Comprehensive Cancer Center Biostatistics Core Facility, NIH grant P30 CA43703), E. Lerzan Ormici and Benigno Rodriguez for help with statistical analysis, and R. Michael Sramkoski and Min Lamh of the Case Comprehensive Cancer Center core facilities for assistance with flow cytometry and fluorescence microscopy.

Abbreviations

Mtb
: *Mycobacterium tuberculosis*

BCG
: *Mycobacterium bovis* strain Bacillus Calmette Guerin

MHC-II
: class II MHC

BCG-GFP
: BCG expressing GFP

BAL
: bronchoalveolar lavage

References

1. Noss EH, Pai RK, Sellati TJ, Radolf JD, Belisle J, Golenbock DT, Boom WH, Harding CV. Toll-like receptor 2-dependent inhibition of macrophage class II MHC expression and antigen processing by 19 kD lipoprotein of *Mycobacterium tuberculosis*. J Immunol 2001;167:910–918. [PubMed: 11441098]
2. Pai RK, Convery M, Hamilton TA, Boom WH, Harding CV. Inhibition of IFN-gamma-induced class II transactivator expression by a 19-kDa lipoprotein from *Mycobacterium tuberculosis*: a potential mechanism for immune evasion. J Immunol 2003;171:175–184. [PubMed: 12816996]
3. Kincaid EZ, Ernst JD. *Mycobacterium tuberculosis* exerts gene-selective inhibition of transcriptional responses to IFN-gamma without inhibiting STAT1 function. J Immunol 2003;171:2042–9. [PubMed: 12902509]
4. Noss EH, Harding CV, Boom WH. *Mycobacterium tuberculosis* inhibits MHC class II antigen processing in murine bone marrow macrophages. Cell Immunol 2000;201:63–74. [PubMed: 10805975]
5. Fulton SA, Reba SM, Pai RK, Pennini M, Torres M, Harding CV, Boom WH. Inhibition of major histocompatibility complex II expression and antigen processing in murine alveolar macrophages by *Mycobacterium bovis* BCG and the 19-kilodalton mycobacterial lipoprotein. Infect Immun 2004;72:2101–10. [PubMed: 15039332]
6. Gehring AJ, Rojas RE, Canaday DH, Lakey DL, Harding CV, Boom WH. The *Mycobacterium tuberculosis* 19-kilodalton lipoprotein inhibits gamma interferon-regulated HLA-DR and Fc gamma R1 on human macrophages through Toll-like receptor 2. Infect Immun 2003;71:4487–97. [PubMed: 12874328]
7. Pai RK, Pennini ME, Tobian AA, Canaday DH, Boom WH, Harding CV. Prolonged toll-like receptor signaling by *Mycobacterium tuberculosis* and its 19-kilodalton lipoprotein inhibits gamma interferon-induced regulation of selected genes in macrophages. Infect Immun 2004;72:6603–14. [PubMed: 15501793]
8. Ting LM, Kim AC, Cattamanchi A, Ernst JD. *Mycobacterium tuberculosis* inhibits IFN-gamma transcriptional responses without inhibiting activation of STAT1. J Immunol 1999;163:3898–906. [PubMed: 10490990]
9. Gehring AJ, Dobos KM, Belisle JT, Harding CV, Boom WH. *Mycobacterium tuberculosis* LprG (Rv1411c): A novel TLR-2 ligand that inhibits human macrophage class II MHC antigen processing. J Immunol 2004;173:2660–8. [PubMed: 15294983]

10. Pecora ND, Gehring AJ, Canaday DH, Boom WH, Harding CV. *Mycobacterium tuberculosis* LprA is a lipoprotein agonist of TLR2 that regulates innate immunity and APC function. J Immunol 2006;177:422–9. [PubMed: 16785538]
11. Fortune SM, Solache A, Jaeger A, Hill PJ, Belisle JT, Bloom BR, Rubin EJ, Ernst JD. *Mycobacterium tuberculosis* inhibits macrophage responses to IFN-gamma through myeloid differentiation factor 88-dependent and -independent mechanisms. J Immunol 2004;172:6272–80. [PubMed: 15128816]
12. Pennini ME, Pai RK, Schultz DC, Boom WH, Harding CV. *Mycobacterium tuberculosis* 19-kDa lipoprotein inhibits IFN-gamma-induced chromatin remodeling of MHC2TA by TLR2 and MAPK signaling. J Immunol 2006;176:4323–30. [PubMed: 16547269]
13. Hamerman JA, Aderem A. Functional transitions in macrophages during in vivo infection with *Mycobacterium bovis* bacillus Calmette-Guerin. J Immunol 2001;167:2227–33. [PubMed: 11490009]
14. Gonzalez-Juarrero M, Shim TS, Kipnis A, Junqueira-Kipnis AP, Orme IM. Dynamics of macrophage cell populations during murine pulmonary tuberculosis. J Immunol 2003;171:3128–35. [PubMed: 12960339]
15. Valdivia RH, Hromockyj AE, Monack D, Ramakrishnan L, Falkow S. Applications for green fluorescent protein (GFP) in the study of host-pathogen interactions. Gene 1996;173:47–52. [PubMed: 8707055]
16. Sklar MD, Tereba A, Chen BD, Walker WS. Transformation of mouse bone marrow cells by transfection with a human oncogene related to c-myc is associated with the endogenous production of macrophage colony stimulating factor 1. J Cell Physiol 1985;125:403–12. [PubMed: 3877730]
17. Humphreys IR, Stewart GR, Turner DJ, Patel J, Karamanou D, Snelgrove RJ, Young DB. A role for dendritic cells in the dissemination of mycobacterial infection. Microbes Infect 2006;8:1339–46. [PubMed: 16697232]
18. Kuchtey J, Fulton SA, Reba SM, Harding CV, Boom WH. Interferon-alpha-beta mediates partial control of early pulmonary *Mycobacterium bovis* bacillus Calmette-Guerin infection. Immunology 2006;118:39–49. [PubMed: 16630021]
19. Fulton SA, Martin TD, Redline RW, Henry Boom W. Pulmonary immune responses during primary *Mycobacterium bovis*- Calmette-Guerin bacillus infection in C57BL/6 mice. Am J Respir Cell Mol Biol 2000;22:333–343. [PubMed: 10696070]
20. Dunn PL, North RJ. Virulence ranking of some *Mycobacterium tuberculosis* and *Mycobacterium bovis* strains according to their ability to multiply in the lungs, induce lung pathology, and cause mortality in mice. Infect Immun 1995;63:3428–37. [PubMed: 7642273]
21. Reljic R, Di Sano C, Crawford C, Dieli F, Challacombe S, Ivanyi J. Time course of mycobacterial infection of dendritic cells in the lungs of intranasally infected mice. Tuberculosis 2005;85:81–8. [PubMed: 15687031]
22. Roederer M, Murphy RF. Cell-by-cell autofluorescence correction for low signal-to-noise systems: application to epidermal growth factor endocytosis by 3T3 fibroblasts. Cytometry 1986;7:558–65. [PubMed: 3096673]
23. Wolf AJ, Linas B, Trevejo-Nunez GJ, Kincaid E, Tamura T, Takatsu K, Ernst JD. *Mycobacterium tuberculosis* infects dendritic cells with high frequency and impairs their function *in vivo*. J Immunol 2007;179:2509–2519. [PubMed: 17675513]
24. Pennini ME, Liu Y, Yang J, Croniger CM, Boom WH, Harding CV. CCAAT/enhancer-binding protein beta and delta binding to CIITA promoters is associated with the inhibition of CIITA expression in response to *Mycobacterium tuberculosis* 19-kDa lipoprotein. J Immunol 2007;179:6910–8. [PubMed: 17982082]
25. Ordway D, Henao-Tamayo M, Orme IM, Gonzalez-Juarrero M. Foamy macrophages within lung granulomas of mice infected with *Mycobacterium tuberculosis* express molecules characteristic of dendritic cells and antiapoptotic markers of the TNF receptor-associated factor family. J Immunol 2005;175:3873–81. [PubMed: 16148133]
26. Pedroza-Gonzalez A, Garcia-Romo GS, Aguilar-Leon D, Calderon-Amador J, Hurtado-Ortiz R, Orozco-Estevez H, Lambrecht BN, Estrada-Garcia I, Hernandez-Pando R, Flores-Romo L. In situ analysis of lung antigen-presenting cells during murine pulmonary infection with virulent *Mycobacterium tuberculosis*. Int J Exp Pathol 2004;85:135–45. [PubMed: 15255967]

27. Kincaid EZ, Wolf AJ, Desvignes L, Mahapatra S, Crick DC, Brennan PJ, Pavelka MS Jr, Ernst JD. Codominance of TLR2-dependent and TLR2-independent modulation of MHC class II in *Mycobacterium tuberculosis* infection in vivo. J Immunol 2007;179:3187–95. [PubMed: 17709534]

28. Ben-Ali M, Barbouche MR, Bousnina S, Chabbou A, Dellagi K. Toll-like receptor 2 Arg677Trp polymorphism is associated with susceptibility to tuberculosis in Tunisian patients. Clin Diagn Lab Immunol 2004;11:625–6. [PubMed: 15138193]

29. Bochud PY, Hawn TR, Aderem A. Cutting edge: a toll-like receptor 2 polymorphism that is associated with lepromatous leprosy is unable to mediate mycobacterial signaling. J Immunol 2003;170:3451–4. [PubMed: 12646604]

30. Ogus AC, Yoldas B, Ozdemir T, Uguz A, Olcen S, Keser I, Coskun M, Cilli A, Yegin O. The Arg753GLn polymorphism of the human toll-like receptor 2 gene in tuberculosis disease. Eur Respir J 2004;23:219–23. [PubMed: 14979495]

31. Drennan MB, Nicolle D, Quesniaux VJ, Jacobs M, Allie N, Mpagi J, Fremond C, Wagner H, Kirschning C, Ryffel B. Toll-like receptor 2-deficient mice succumb to *Mycobacterium tuberculosis* infection. Am J Pathol 2004;164:49–57. [PubMed: 14695318]

32. Reiling N, Holscher C, Fehrenbach A, Kroger S, Kirschning CJ, Goyert S, Ehlers S. Cutting edge: toll-like receptor (TLR)2- and TLR4-mediated pathogen recognition in resistance to airborne infection with *Mycobacterium tuberculosis*. J Immunol 2002;169:3480–4. [PubMed: 12244136]

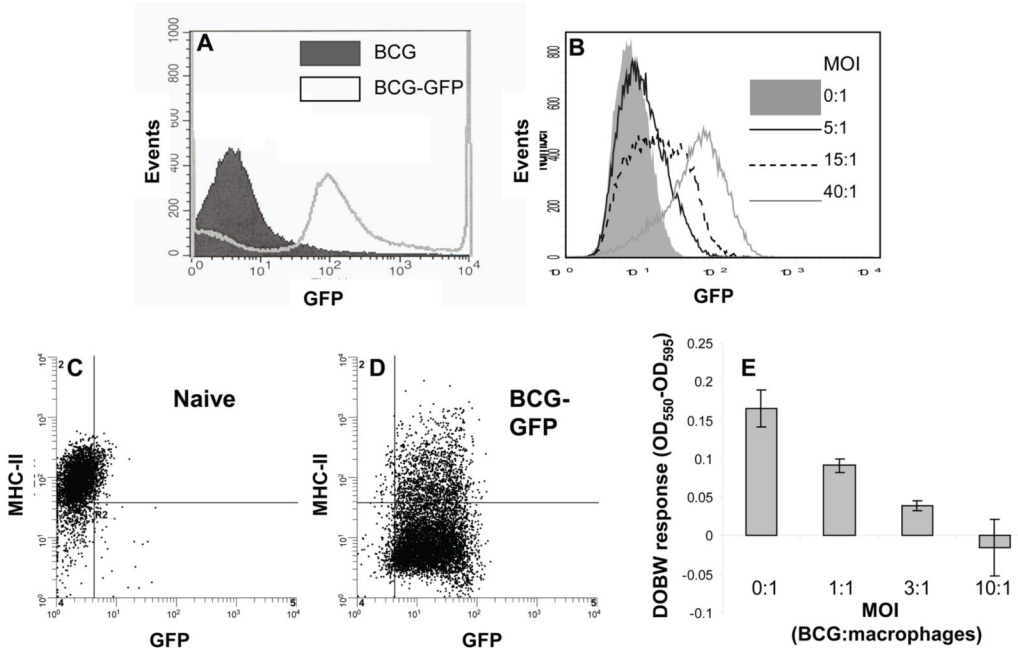

Figure 1. BCG-GFP is detectable by flow cytometry and down-regulates surface expression of MHC-II and antigen processing and presentation by bone marrow-derived macrophages

A. *M. bovis*-BCG ("BCG") was transformed with the GFP-expressing plasmid pMV262 to produce BCG-GFP. GFP fluorescence was 20-fold higher for BCG-GFP than non-transformed BCG. B. Murine bone marrow-derived macrophages were incubated with control medium (MOI of 0:1) or BCG-GFP at varying MOI (bacteria: macrophages) for 48 h (2 ng/ml IFN-gamma was present for the final 24 h). C and D. MHC-II expression by macrophages from panel B that were uninfected (C) or infected at MOI of 40:1 (D). E. Macrophages were incubated with BCG-GFP and IFN-gamma as in panel B and then incubated with 500 μg/ml OVA for 2 h, fixed, and incubated with DOBW T hybridoma cells. IL-2 was assessed in supernatants with a colorimetric CTLL-2 bioassay to determine presentation of processed OVA. Results are expressed as means of triplicate wells ± SD. When error bars are not visible, they are smaller than the symbol width.

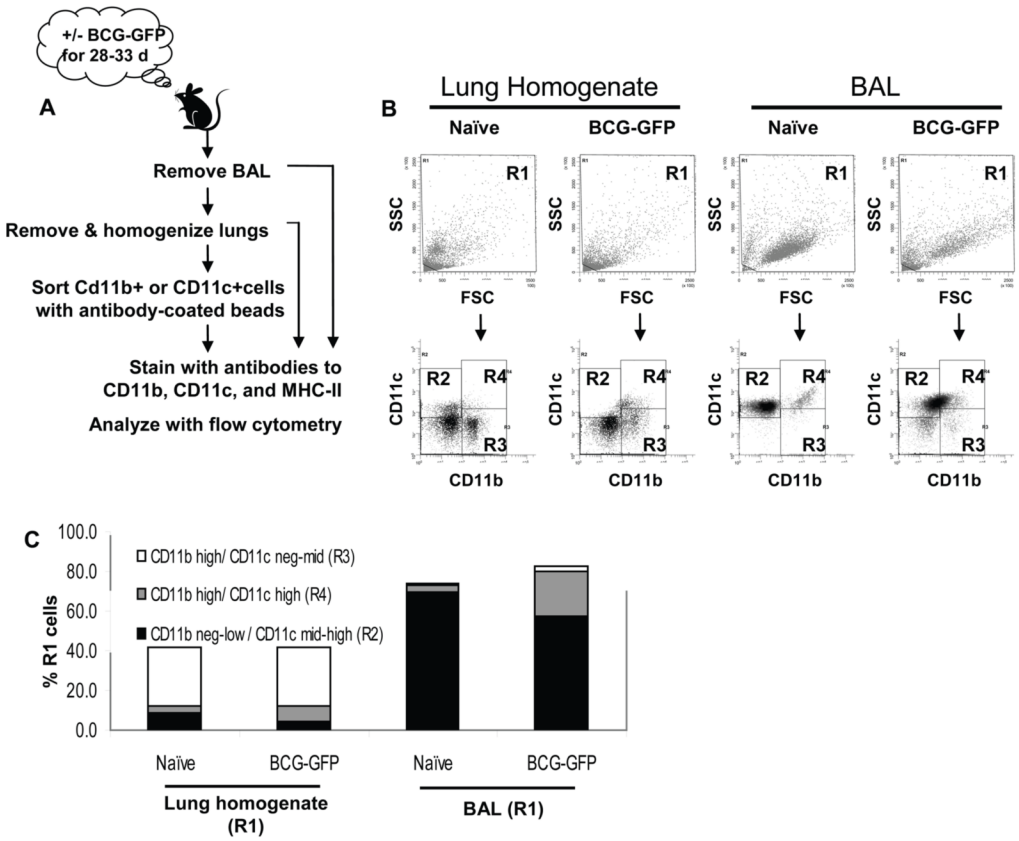

Figure 2. Definition of lung APC subsets by differing expression of CD11b and CD11c

C57BL/6J mice were aerosol-infected with BCG-GFP for 28–33 d. Lungs were lavaged to obtain BAL cells, perfused with PBS and homogenized. Lung homogenate was analyzed directly or used to prepare CD11b or CD11c affinity-sorted cells. Cells were stained for CD11b, CD11c and MHC-II. Fig. 2 shows flow cytometry analysis of lung homogenate, but all other figures show analysis of CD11b or CD11c affinity-sorted cells, which provide lower autofluorescence background for studies to detect BCG-GFP+ events. A. Sample preparation schematic. B. Dot plots showing forward scatter (FSC) vs. side scatter (SSC) and CD11b vs. CD11c for naïve and BCG-GFP-infected lung homogenate and BAL. The R1 gate was drawn on FSC vs. SSC plots to exclude only subcellular debris in the lower left corner. Cells from R1 were analyzed for CD11b and CD11c to define 3 major APC populations (R2, R3 and R4 gates, see Table 1). C. Mean percentage of R1 cells represented by each APC subsets in lung homogenate and BAL from naïve and BCG-GFP-infected mice. Data was drawn from 3–4 experiments with 2–5 mice per group.

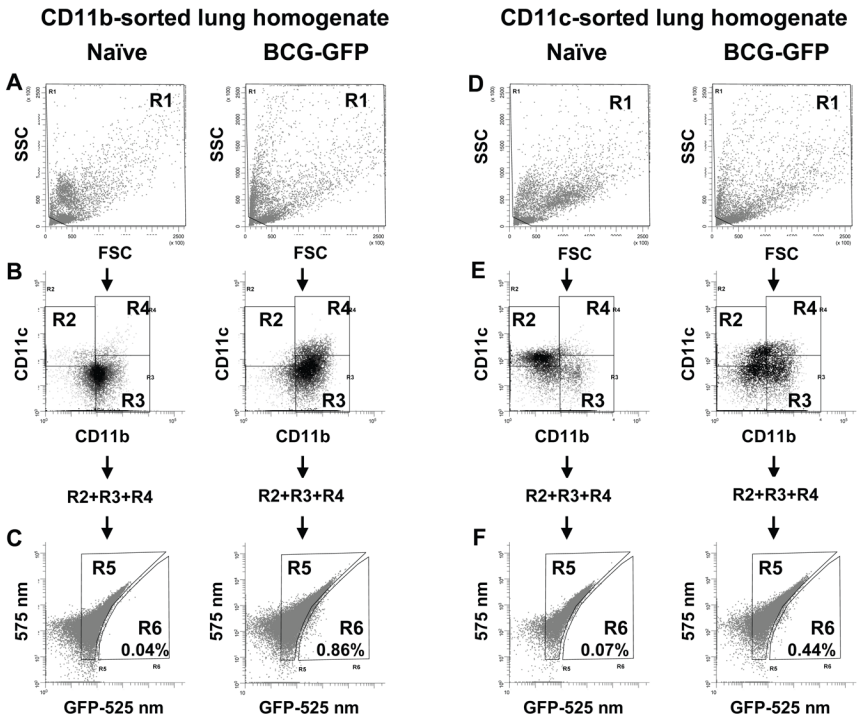

Figure 3. Detection of BCG-GFP *ex vivo* by flow cytometry of lung APCs

CD11b or CD11c affinity-sorted lung APCs were prepared from naïve or BCG-GFP-infected mice. A, D. R1 gate defined by FSC vs. SSC. B, E. Gates R2, R3 and R4 defined by CD11b vs. CD11c expression on cells from R1. C, F. Cells from total lung APCs (R2 + R3 + R4) analyzed for fluorescence at 525 nm (autofluorescence + GFP signal) vs. 575 nm (autofluorescence). BCG-GFP+ events are right-shifted on the *x*-axis (525 nm), placing them in gate R6, whereas GFP− events are included in gate R5. Mice infected with non-fluorescent BCG had background numbers of events in R6 that were similar to those of naïve mice (data not shown). Percentages represent R6/(R2 + R3 + R4) and are from a representative experiment.

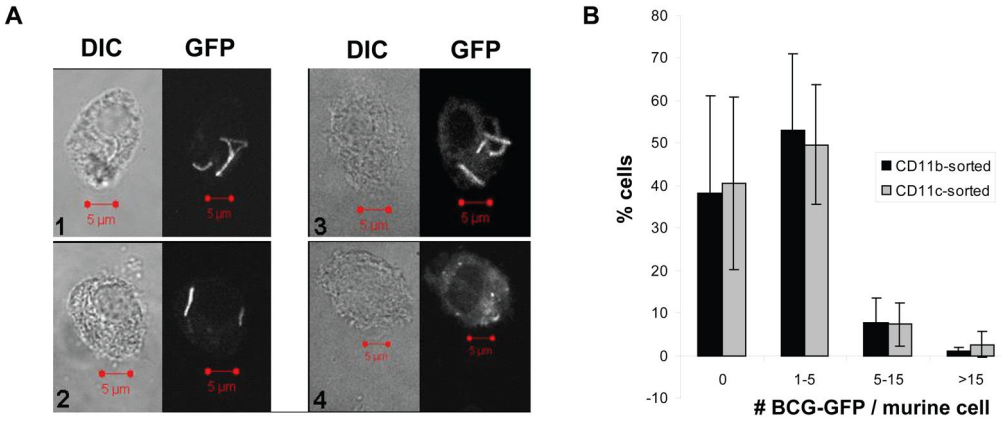

Figure 4. Fluorescence microscopy of BCG-GFP+ cells obtained by FACS

A. Paired differential interference contrast (DIC) and fluorescence microscopy (GFP) images of cells from the R6 gate that contained BCG-GFP (panels 1–3) and one example (panel 4) of a highly autofluorescent cell with granules that represents an apparent false GFP+ event (4). Bars = 5 microns. B. Cells from gate R6 were scored by fluorescence microscopy for the number of mycobacteria/cell. Each data point represents the mean +/− SD from 3 independent experiments (50–225 cells were scored for each experiment).

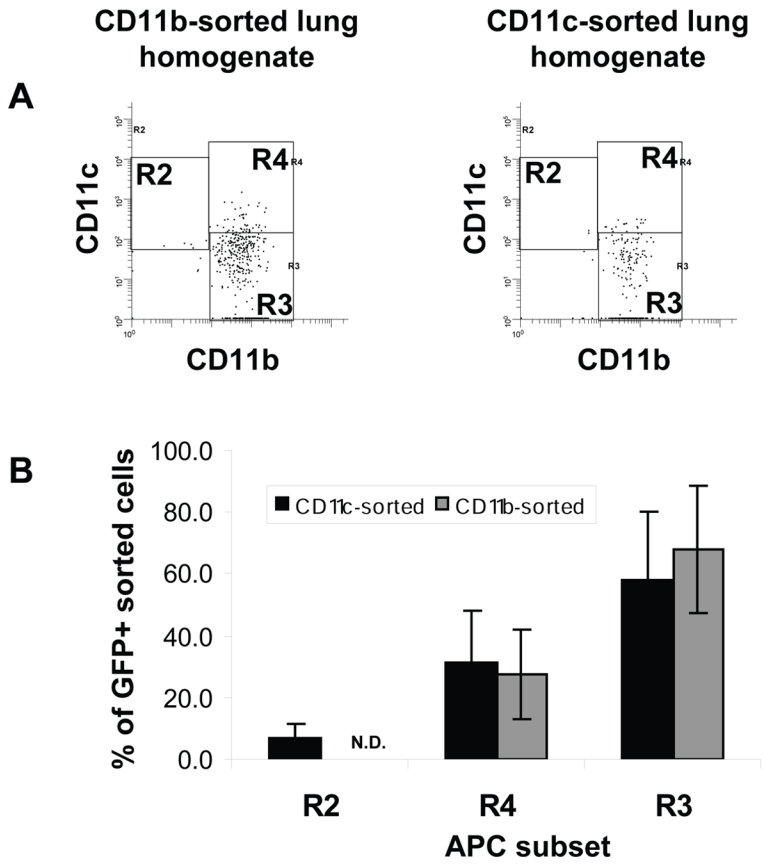

Figure 5. BCG-GFP is most often found in CD11b^{high}/CD11c$^{neg\text{-}mid}$ cells

CD11b or CD11c affinity-sorted cells were prepared from naïve or BCG-GFP-infected lungs. APC subsets were defined as in Fig. 3. GFP+ (R6) events were selected for analysis (R6 events were drawn from R2 + R3 + R4). A. CD11b vs. CD11c expression by GFP+ cells from a single experiment (affinity-sorted cells pooled from 5 naïve or infected mice). B. Proportion of GFP + (R6) cells in each APC subset (CD11b$^{neg\text{-}low}$/CD11c$^{mid\text{-}high}$, gate R2; CD11b^{high}/CD11c$^{neg\text{-}mid}$, gate R3; CD11b^{high}/CD11c^{high}, gate R4). Each data point represents mean +/− SD of 3 independent experiments (each with cells pooled from 2–5 naïve or infected mice). n.d., not determined (CD11b affinity-sorted cells did not consistently provide sufficient R2 events for analysis of GFP+ events).

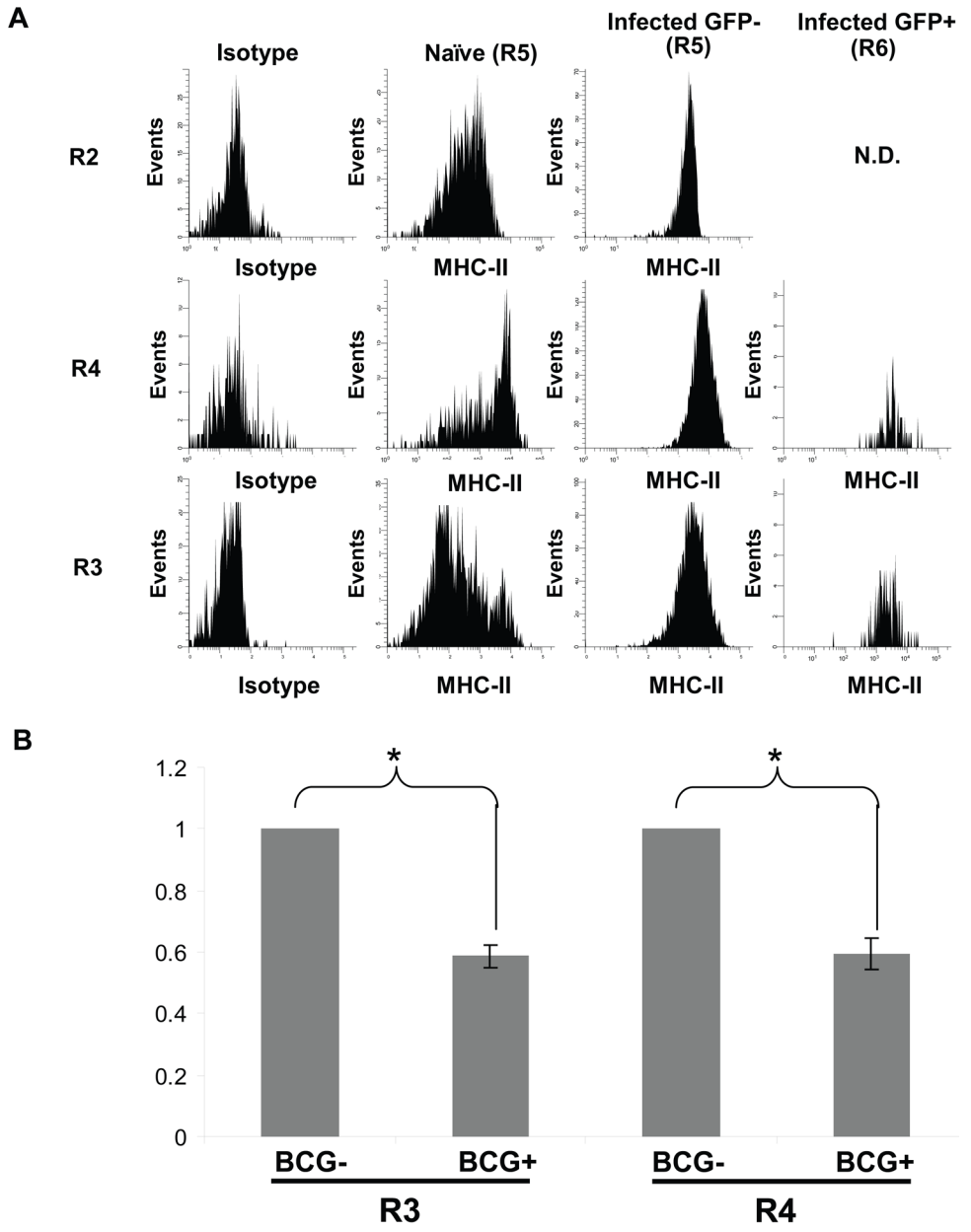

Figure 6. Pulmonary infection increases mean MHC-II expression on lung APCs, but MHC-II is decreased on APCs that harbor mycobacteria

CD11b or CD11c affinity-sorted cells were prepared from naïve or BCG-GFP-infected lungs. APC subsets were defined as in Fig. 3. $CD11b^{neg\text{-}low}/CD11c^{mid\text{-}high}$ cells were analyzed from CD11c affinity-sorted cells; $CD11b^{high}/CD11c^{high}$ and $CD11b^{high}/CD11c^{neg\text{-}mid}$ cells were analyzed from CD11b affinity-sorted cells (n.d. = not determined due to insufficient number of infected cells). A. Isotype control antibody staining (gray filled curve) or anti-MHC-II staining of BCG-GFP− (R5) APCs and BCG-GFP+ (R6) APCs from the same infected lungs. Each sample represents cells pooled from 5 mice. MFI for MHC-II is indicated on each histogram. B. MHC-II fold-change between BCG-GFP− and BCG-GFP+ cells in R3 and R4 from the same infected lungs. Data has been normalized to BCG-GFP+ samples. Data represents the average of 3–4 experiments, each containing cells pooled from 5–10 mice. Asterisks (*) indicate statistical significance ($p < 0.05$) as determined by *t* test (see Methods).

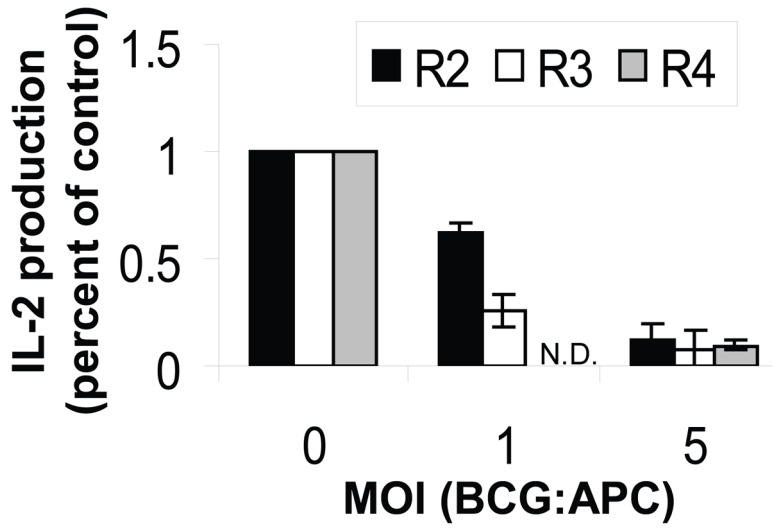

Figure 7. MHC-II antigen processing and presentation by purified lung APCs is inhibited by in vitro infection with BCG-GFP

Alveolar macrophages (R2), lung macrophages (R3) and lung DCs (R4) were purified by FACS from naïve BALB/c mice and infected with BCG-GFP for 48 h with IFN-gamma (4 ng/ml) present during the final 24 h. Soluble OVA (1 mg/ml) was then added for 24 h, and the APCs were fixed and processed for detection of OVA presentation to DOBW T hybridoma cells. IL-2 production was determined by ELISA. Data represent pooled results of two independent experiments expressed as percent of control IL-2 production observed with each uninfected APC type. Data points represent the mean of four results (two for DCs). DC data were obtained only at MOI of 0 and 5 due to limiting cell numbers. N.D. = not determined.

Table 1

Summary of lung cell subsets

Cell subset name	Flow cytometry gate parameters	Gate name
Total lung cells *1	Scatter exclusion of subcellular debris	R1
CD11b or CD11c affinity-sorted cells *2	Scatter exclusion of subcellular debris	R1
Alveolar macrophages *3	$CD11b^{neg\text{-}low}/CD11c^{mid\text{-}high}$	R2
DCs *3	$CD11b^{high}/CD11c^{high}$	R4
Lung macrophages *3	$CD11b^{high}/CD11c^{neg\text{-}mid}$	R3
Total lung APCs	R2 + R3 + R4	R2 + R3 + R4

*1 Used only for studies that did not assess GFP+ events. R1-gated total lung homogenate. The R1 gate contains all events except those that represent subcellular debris based on optical scatter analysis.

*2 Used for all studies that assessed GFP+ events. Cells were derived from total lung homogenate by immunoaffinity bead sorting, and subcellular debris was excluded with the R1 gate.

*3 Lung APC subset definitions adapted from Gonzalez-Juarrero [14]. R2, R3 and R4 events were derived from R1-gated total lung homogenate or R1-gated CD11b or CD11c affinity-sorted cells.

Table 2

Efficiency of flow cytometry for detection of BCG-GFP+ events from murine lung tissue[*1]

	Percent APCs containing BCG-GFP by flow cytometry	Percent affinity-sorted cells containing BCG-GFP by flow cytometry	CFU/affinity-sorted cells	Detection efficiency
Formula[*2]	mean (R6/(R2 + R3 + R4))	mean (R6′/R1)	mean (CFU/R1)	mean (R6′/CFU)
CD11b affinity-sorted cells	0.60 +/− 0.21%	0.29 +/− 0.18%	0.9 +/− 0.56%	38 +/− 0.17%
CD11c affinity-sorted cells	0.52 +/− 0.26%	0.35 +/− 0.22%	1.1 +/− 0.47%	42 +/− 0.37%

[*1]Data are shown as mean +/− SD. Data are from 3 separate experiments with 2–5 mice per group (pooled to generate CD11b or CD11c affinity-sorted samples).

[*2]R6 events in column 2 are BCG-GFP+ events derived from R2 + R3 + R4, and the proportion of lung APCs that were BCG-GFP+ was determined as R6/(R2 + R3 + R4). For CFU determination, samples were taken from total CD11b or CD11c affinity-sorted cell preparations and included cells both inside and outside R2 + R3 + R4 (strictly represented by R0 events and effectively represented by the R1 gate that excludes only subcellular debris), necessitating comparison of CFU to BCG-GFP+ events derived from R1 (not just R2 + R3 + R4). Therefore, R6′ events in columns 3 and 5 are BCG-GFP+ events derived from R1. CFU values were determined by culture of affinity-sorted cells. R1 was determined by flow cytometry analysis in column 3 and by cell count with a hemacytometer in column 4. Detection efficiency was calculated as mean (R6′/CFU) as opposed to (mean R6′/R1)/(mean CFU/R1).